Thin Solid Films 519 (2011) 5955–5961

Contents lists available at ScienceDirect

Thin Solid Films

journal homepage: www.elsevier.com/locate/tsf

Local thermal-mechanical analysis of ultrathin interfacially mixed poly(ethylene oxide)/poly(acrylic acid) layer-by-layer electrolyte assemblies

Xianke Gu [a,b], Daniel B. Knorr Jr. [a], Guojian Wang [b], René M. Overney [a,*]

[a] Department of Chemical Engineering, University of Washington, Seattle, WA 98115–1750, USA
[b] School of Materials Science and Engineering, Tongji University, Shanghai 200092, China

ARTICLE INFO

Article history:
Received 30 July 2010
Received in revised form 15 March 2011
Accepted 15 March 2011
Available online 31 March 2011

Keywords:
Poly(ethylene oxide)
Poly(acrylic acid)
Layer-by-layer
Scanning force microscopy
Shear modulation force microscopy
Ion conductivity
Organic batteries
Glass transition

ABSTRACT

Ion conductivities of layer-by-layer (LBL) assemblies of solid thin film polyelectrolyte systems involving poly (ethylene oxide) (PEO) and poly(acrylic acid) (PAA) were found to be a strong function of the number of bilayer stacks, n, with conductivities approaching 10^{-7} S/cm for $n<10$, compared to 10^{-9} S/cm for $n\geq 10$ and 10^{-10} S/cm for bulk PEO. Increased ion conductivity for low LBL stack numbers ($n<10$) originated to part from an effective suppression of the PEO crystallization via PEO/PAA blending, which could be inferred from local glass transition temperature measurements involving shear modulation force microscopy. Another phenomenon responsible for high conductivity in thin films was found in the in-plane phase heterogeneity of PEO and PAA. Increased ion conductivity for larger LBL stacks ($n\geq 10$) were attributed to low concentration autoblending caused by PEO-PAA hydrogen bonding, and an average layer thickness of noticeably less than 100 nm. The effect of interfacial constraints was evident in the degree of intermixing, addressed by a thin film extended Fox blend analysis, in the glass and melting transitions of PEO and PAA pure film components. While the glass transition value of PAA decreased by 55% to 46 °C for an 8 nm film, the melting transition for PEO decreased by 15% to 64 °C caused by surface tension effects.

1. Introduction

Poly(ethylene oxide) (PEO) is employed extensively as an electrolyte component in solid state rechargeable lithium batteries because of its excellent complexation properties, such as high flexibility and mechanical stability up to its melting point [1]. In its solid amorphous state, the local relaxation and segmental motion of PEO promote ionic conductivity. Unfortunately, the low melting temperature of pure PEO and its tendency to crystallize limit its use in electronic applications [2]. To increase the ionic conductivity, high glass transition PEO materials with "glassy" matrices [3], crosslinking to achieve high density, or low PEO content polymer stacked film systems have been considered [4,5]. One of the major objectives in using a polymer matrix is to influence the material phase and structural behavior by imposing interfacial constraints. This concept of engineering by imposing constraints on the nanoscale is widely utilized in ultrathin film applications [6]. A way to scale these efforts up is, for instance, by layer-by-layer (LBL) deposition [7–9]. The LBL method offers control and tunability of material properties and architecture at the nanometer scale [10].

Recently, the LBL deposition method has been employed to produce heterogeneous stacks of thin film batteries and fuel cell membranes [11–13] via alternating deposition of PEO and poly (acrylic acid) (PAA) layers from aqueous solutions [11], which utilizes complementary hydrogen bond donor and acceptor interactions [14,15]. Although the conductivity, thermal and mechanical properties of PEO/PAA LBL bulk films have been explored by conventional tools, i.e. differential scanning calorimetry and dynamic mechanical analysis, in previous studies [4], the performance of films with low stack numbers has not been explored. Specifically, since interfacial constraints are known to influence material and local properties for other polymer systems, one may expect the performance and stack growth of ultrathin PEO/PAA LBL films to be influenced by the substrate. This understanding is critical for the design of LBL based technologies, such as LBL electrolytes for solid ultrathin film battery applications.

Based on recent findings of the relatively high ion conductivity of 10^{-9} S/cm in PEO/PAA LBL systems that were attributed to phase blending [4,5], we explore interfacially constrained ultrathin PEO and PAA films, PEO-PAA blends and PEO/PAA LBL assemblies. Of particular interest is the degree of phase intermixing during LBL stacking. This study involves local probe techniques, such as lateral force microscopy (LFM) and shear modulation force microscopy (SM-FM), which provide insight into lateral phase heterogeneities,

* Corresponding author.
E-mail address: roverney@u.washington.edu (R.M. Overney).

0040-6090/$ – see front matter © 2011 Elsevier B.V. All rights reserved.
doi:10.1016/j.tsf.2011.03.039

local glass and melting transitions as a function of the film stacking number.

2. Experimental section

2.1. Materials and sample preparation

Nonionic PEO (4000 kM_w, Polysciences) and polyanionic PAA (90 kM_w, 50 wt.% water solution, Carbemer Inc.) were used as received. The polymers were weighed and dissolved in Millipore filtered water (18 MΩ·cm), and the resultant solutions were pH adjusted to a pH of 2.5 with dilute aqueous HCl. The PEO solution was stirred for 24 h to ensure complete dissolution. All polymer solutions were 0.020 M with respect to repeat unit.

Silicon wafers (thickness 585–610 μm from Addison Engineering, Inc. San Jose, CA) and indium-doped tin oxide (ITO) coated glass substrates (15 mm × 15 mm from Thin Film Devices, Inc.) were used as LBL substrates. ITO film resistance was measured to be 100 Ω/m^2. Substrates were cleaned by ultrasonication (Model 08849, Cole-Parmer Instrument Company) in a series of solvents for 15 min each, in the following order: acetone, methanol, and filtered water. Following the water cleansing, the substrates were dried under a jet of desiccated nitrogen gas. Immediately before use, substrates were cleaned in UV for 20 min.

In a typical LBL assembly, a clean ITO coated glass substrate was immersed for 10 min in PEO (0.020 M H_2O solution), followed by a 10 min immersion into PAA (0.020 M H_2O solution), then another 10 min back in PEO. After each step the sample was rinsed for 2 min, 1 min, and then 1 min in 3 separate beakers filled with water, respectively. This sequence (referred to in the following as a bilayer) after being repeated n times produced a $(PEO/PAA)_n$ composite film. After assembly, all films were dried at 110 °C for 24 h, which has been shown to effectively remove water from LBL assembled films [16].

Pure PEO, pure PAA, and PEO-PAA blend films were spin-casted on a silicon wafer from chloroform or water solutions. Bulk (>300 nm) films of PEO/PAA blends were spun cast from solutions of different ratios of PEO and PAA. Pure PEO and pure PAA were spun cast to different thicknesses (19 nm–135 nm and 8 nm–380 nm, respectively) from a solution of PEO in chloroform and PAA in water, respectively. Pure PEO films were annealed at 70 °C, while pure PAA and PEO/PAA blend films were annealed at 110 °C in a vacuum oven for over 12 h.

2.2. Characterization

2.2.1. Conductivity

After assembly of the LBL films on ITO coated glass, gold electrodes were deposited on the surface of the sample with an Angstrom gold deposition system. This process created two-electrode 3.14 mm^2 test beds in which the LBL assembled films were sandwiched between ITO and gold electrodes. The substrate dimensions allowed 16 such cells per substrate. Ionic conductivity was evaluated by impedance spectroscopy, which was performed using an HP 4192A LF impedance analyzer (5 Hz to 10 MHz). The signal amplitude was 100 mV excluding the bias. Conductivity measurements were conducted in an environmental chamber at approximately 50% relative humidity. Impedance data of materials that have capacitive and resistive components, when represented in the Nyquist diagram (i.e., the negative of the imaginary part in the y axis and the real part in the x axis—each point corresponding to a different frequency), lead to a succession of semicircles. The second intercept of the high frequency semi-circle with the real axis is the resistance (R_b) of the sample. Hence, the conductivity (σ_b) is written

$$\sigma_b = 1 / R_b \times l / A, \quad (1)$$

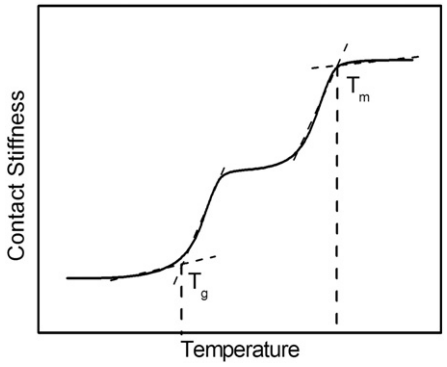

Fig. 1. Illustration of a contact stiffness SM-FM plot revealing both the glass transition temperature T_g at the onset of change, and the melting temperature at the completion of the melting process. The signal saturation in T right after T_g reflects the time necessary for the probing tip to achieve pressure equilibrium in a medium that behaves very sluggishly close to the glass transition.

where l is the thickness and A is the area of the electrode deposited on the sample [17].

2.2.2. Local analyses

Shear modulation force microscopy (SM-FM) [18,19], lateral force microscopy (LFM), [20] and scanning force microscopy (SFM) were employed to determine the glass transition properties of the layers in the primary stack material, evaluate local phase heterogeneities and material analysis, and probe the topography of the films, respectively. Local analyses were conducted with a scanning probe microscope (Topometrix Explorer, Veeco, CA) with contact mode cantilever sensors (PPP-CONT, Nanosensors, nominal and lateral spring constants of ~0.2 N/m and 80 N/m, respectively). Film thicknesses were determined with a conventional SFM (EasyScan 2, Nanosurf AG, Switzerland). This involved razor blade scratching of the films, a method that has been verified with profilometry involving thicker films.

SM-FM is a non-scanning method used to study structural transitions and thermally induced relaxations. *Briefly*: A nanometer sharp SFM cantilever tip is brought into contact with the sample surface [18]. While a constant load is applied, the probing tip is laterally modulated with a “no-slip” nanometer amplitude. The modulation response signal, a measure of the contact stiffness, is analyzed. The kinks indicate critical temperatures of transitions in the material. Fig. 1 illustrates the qualitative behavior of a SM-FM curve, and the location that defines the glass transition and melting temperature. While the glass transition temperature is taken at the onset of change, the melting temperature is taken at the completion of the transition process.

3. Results and discussion

3.1. Growth and ionic conductivity of ultrathin layer-by-layer films

We will start this section with a quite interesting finding concerning the ion-conductivity in ultrathin films, which was accompanied by a qualitative change in the thickness growth profile. As illustrated in Fig. 2, the thickness of $(PEO/PAA)_n$ stacked LBL films, determined by SFM, revealed exponential growth up to a stacking number of $n = 8$, followed by linear growth. Linear growth behavior has also been reported for other polyelectrolyte multilayer systems [21]. In exponential growth region ($n < 8$), the fit exponential equation could be obtained as shown in Eq. (2)

$$t = 8.28 \times exp^{\left(\frac{n}{2.28}\right)} \quad (2)$$

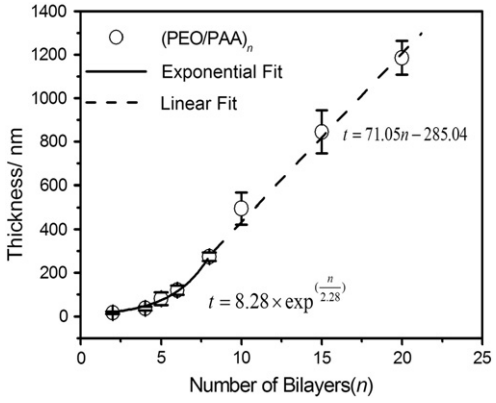

Fig. 2. Thickness growth of $(PEO/PAA)_n$ as function of the number of bilayers. Both the exponential and linear exhibit an R^2-value of 0.99.

where t is the total thickness and n is the number of bilayers of the LBL films. Furthermore, when the number of bilayers is up to 8 ($n>8$), the fit linear equation could be obtained as:

$$t = 71.05n - 285.04 \quad (3)$$

The average PEO/PAA bilayer thickness was determined to be 8.5 nm for two stacks ($n=2$), and 56 nm for $n=40$ (not shown). Interestingly, as shown in Fig. 3, the conductivity of the $(PEO/PAA)_n$ LBL films was found to be a strong function of the number of stacks. At low stack number, n, a high conductivity, on the order of 10^{-7} S/cm is revealed, steadily decreasing to a saturating value of magnitude 10^{-9} S/cm for $n>10$, which is in agreement with that of Hammond's group for thick PEO/PAA LBL films [5], and which exceeds PEO's bulk ion conductivity [22] by at least an order of magnitude in ambient conditions. Considering that up to $n=8$, the growth behavior of the LBL film is exponential, the average single component layer thickness, if compared to stacks of $n>10$, is distinctly smaller than the ~50 nm for $n<10$. If we further reflect on the vast results documented in the open literature [23–28] of the impact of interfacial and dimensional constraints in thin polymer films (<100 nm) on material transport properties, the increased ionic conductivity in Fig. 3 could be attributed to nanoconstraints. In the case of PEO, nanoconstraints may suppress crystallization, which is known to significantly hinder the ionic transport, and this aspect is investigated in greater detail below.

3.2. Ultrathin PEO films and LBL assemblies

Intuitively, as crystallization is the origin for reduced ion conductivity in solid PEO polyelectrolyte systems, it would seem that nanoconfinement may be effectively preventing PEO crystallization in LBL films for low values of n, thereby increasing the conductivity. To determine if this is the case here, silicon oxide wafer supported thin films of PEO were investigated by SFM as a function of film thickness. As evident in Fig. 4(a) which shows small crystallites on the order of tens of nanometers in size, crystallinity is apparent down to thicknesses of 19 nm. Accompanying features, such as small crystal boundaries, are observed for PEO films as thickness with 30 nm in Fig. 4(b). More apparent crystal boundaries are observed for PEO films exceeding ~61 nm (Fig. 4(c–d)). The existence of crystalline phases for ultrathin PEO films is in agreement with previous work [29,30]. Based on these observations, mere dimensional or interfacial constraints, as the reason for crystallinity suppression in LBL systems, are insufficient. For that reason, we investigated the morphology of PEO-PAA LBL systems that are documented in Fig. 5, for $n=2$, 5 and 15.

Simplistically, one would expect that, for a true layer-by-layer assembly process, the top layer consists of PAA alone. However, as shown in previous work [4], it is precarious to assume that the LBL process produces truly laminar phase separated systems. Utilizing lateral force microscopy (LFM)[31,32], where changes in contrast indicate differences in friction coefficient (and therefore in composition), we find that the surfaces of the LBL films are indeed heterogeneous for low stack numbers. Fig. 5(d) shows strong contrast for ultrathin films that can be attributed to PEO-rich (bright contrast), and PAA-rich regions (dark contrast). The contrast is found to progressively vanish for thicker films ($n>\sim10$), Fig. 5(e, f), revealing a single phase, corresponding to a PAA rich blend as found below from SM-FM analysis. This is shown in the friction plot of Fig. 6. Friction forces are known for their sensitivity towards phase distinction [31] and shear property changes within the same phase [33]. Fig. 6 reveals for the top layer of the LBL stacks that their phase behavior divert from the PAA phase (seen as a friction coefficient reduction from $\mu_{PAA}=0.3$) below $n\approx15$.

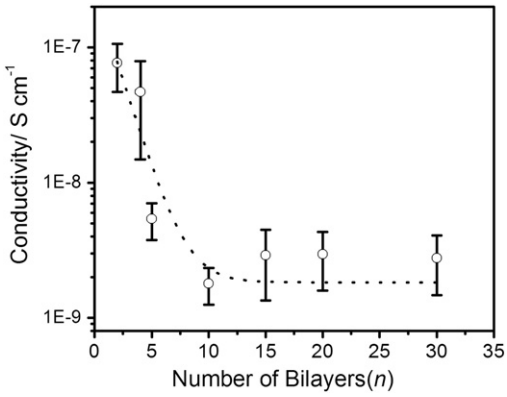

Fig. 3. Conductivity of LBL $(PEO/PAA)_n$ films as a function of number of stacks.

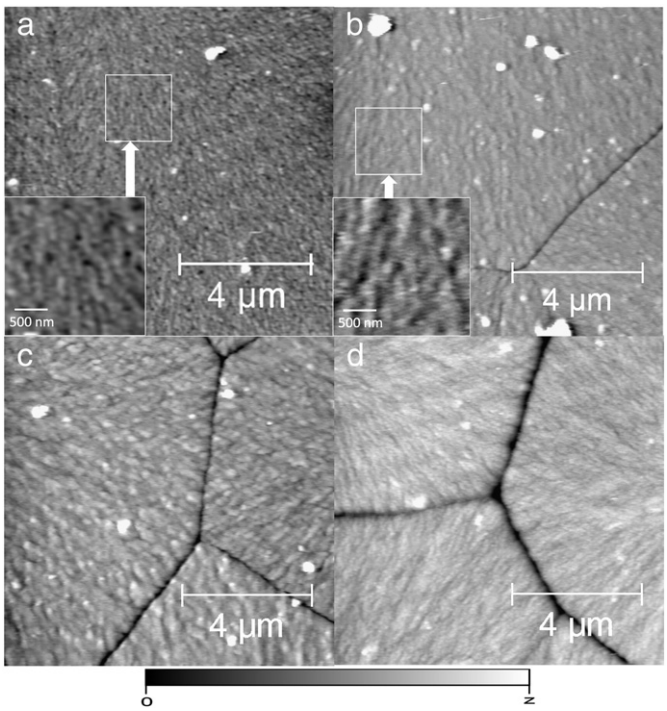

Fig. 4. Contact mode SFM images of PEO films on silicon (deposited via spin-casting) with scan size of 10 μm with varying thicknesses (and height dynamic range z): (a) 19 nm (z = 27 nm), (b) 32 nm (z = 52 nm), (c) 61 nm (z = 34 nm), and (d) 135 nm (z = 77 nm).

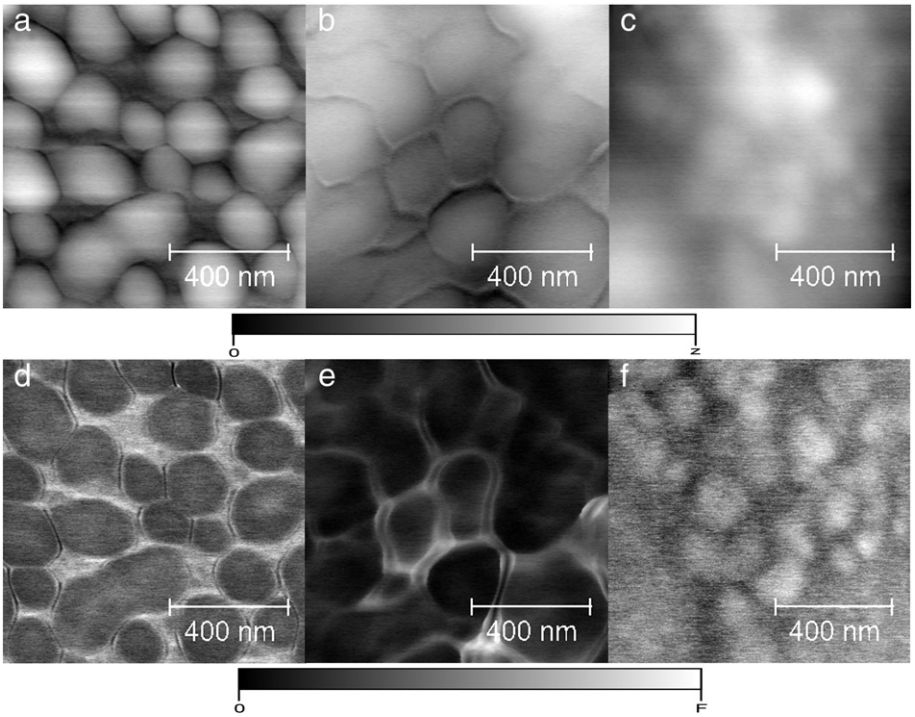

Fig. 5. Topography images (with height dynamic range z) of (a) $(PEO/PAA)_2$ (z = 37 nm), (b) $(PEO/PAA)_5$ (z = 78 nm), and (c) $(PEO/PAA)_{15}$ (z = 34 nm), and composite LFM images (from forward minus reverse scans) (with friction dynamic range z) of (d) $(PEO/PAA)_2$ (z = 14 nN), (e) $(PEO/PAA)_5$ (z = 9 nN), and (f) $(PEO/PAA)_{15}$ (z = 13 nN). (dark) = low friction and (bright) = high friction.

3.3. PEO-PAA blends and LBL assemblies

Given the LFM phase contrast in films of low stack numbers, the LBL fabrication method results in compositional heterogeneities within the film layers, and thus cannot be described as the sequential deposition of uniform layers. This is further illuminated with a local phase analysis involving shear modulation force microscopy (SM-FM) [18]. To obtain a comprehensive picture of the phase behavior, (i) pure PAA films, spin coated from solution, (ii) and spin coated PEO/PAA blends, are contrasted with (iii) PEO/PAA LBL assembled films. At room temperature, bulk PAA is in a glassy state ($T_{g,\ PAA} = 99$ °C) [4], and bulk PEO is in a rubbery or crystalline state ($T_{g,PEO} = -77$ °C) [30].

For pure spin-cast PAA, the glass transition values near the free film surfaces, identified from kinks in the SM-FM curves, Fig. 7(a) (see also Fig. 1), reveal bulk-deviating decreasing values for films with thickness δ<~300 nm. The $T_{g,\ PAA}$ values are presented in Fig. 7(c). Their monotonic behavior with film thickness indicates a structural heterogeneity normal to the film surface, as found for many other substrate constrained polymer systems [23–28].

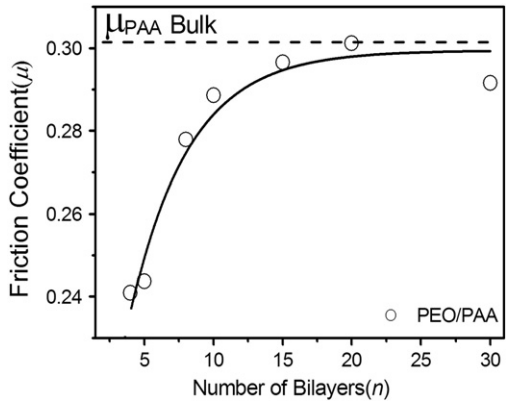

Fig. 6. Friction coefficient vs. number of stacks in LBL films.

For pure spin-cast PEO with a glass transition value far below room temperature, only its melting transitions are observed in the investigated temperature regime, Fig. 7(b). They are found to be slightly thickness dependent reaching the bulk melting transition value [30,34], T_m, of 77 °C at 388 nm. A decrease in the melting transition value, as depicted in Fig. 7(c) for PEO, is well known to occur in small crystals (typically reported for metal clusters), where the surface energy influences the chemical potential [35]. This phenomenon is rarely reported or observed for macromolecular systems, such as polymers.

SM-FM results for spin cast blends of PEO-PAA are provided in Fig. 8(a). They are contrasted to LBL PEO/PAA stacks for $n \in \{5, 40\}$, Fig. 8(b). As expected for the PEO-PAA blends, each film exhibits only one single glass transition that is a strong function of composition. Also the PEO/PAA LBL films exhibit each only one glass transition, which we can conclude to be caused by phase blending during the LBL process, in agreement with earlier findings by Hammond's group [4,5]. Hammond attributed the lack of single temperature transitions (i.e., the lack of melting for PEO and pure phase glass transition for PAA) to hydrogen bonding between PAA and PEO, promoting blending [4]. The blend glass transition in PEO/PAA LBL films dominates the SM-FM study. As discussed for $n = 2$ below, the existence of pure PEO phase within the top layer is possible, however in size small compared to the blend component. Friction results, Fig. 6, conductivity measurements, Fig. 3, and blend concentration results, discussed next, all indicate that the pure phase of PEO decreases with increasing layer number, and vanishes for $n > 12$.

To infer the composition of PEO/PAA LBL films, typically the well known Fox equation, [36] i.e.,

$$\frac{1}{T_{g,PEO/PAA}} = \frac{x_{PAA}}{T_{g,PAA}} + \frac{(1 - x_{PAA})}{T_{g,PEO}}, \tag{4}$$

is employed, which relates in this case the blend glass transition $T_{g,PEO/PAA}$ to the PAA composition concentration, x_{PAA} with $T_{g,PAA} = 99$ °C and $T_{g,PEO} = 77$ °C. We utilized the glass transition values of the PEO/PAA blended films of known compositions, plotted in Fig. 8(a), in

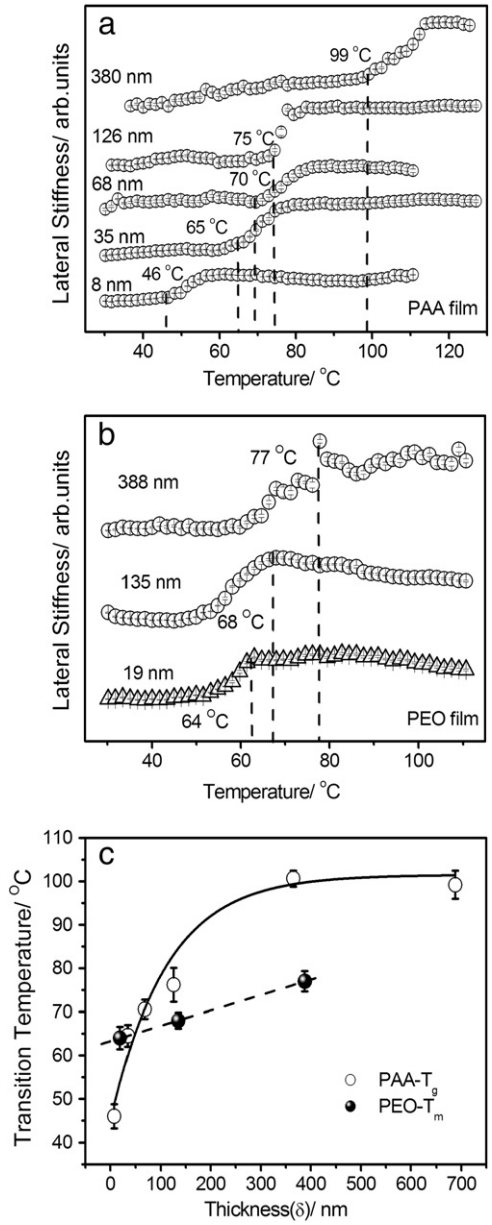

Fig. 7. SM-FM analysis of (a) PAA and (b) PEO for films below 400 nm thickness. (c) Compilation of the transition temperature values from (a) and (b) for PAA (T_g) and PEO (T_m), respectively.

conjunction with Eq. (4), and obtained the Fox fit for PEO/PAA, as depicted with the solid line in Fig. 9(a). Via the Fox fit, we can now assign to each glass transition value of the stacked films its corresponding concentration x_{PAA}, as shown in Fig. 9(a). However, interfacial constraints as observed in blends in Fig. 6 could shift these values.

To assess interfacial constraint effects, we expand the Fox equation by incorporating the film or layer thickness t. We include in Eq. (4) empirical data fits for $T_g = T_g(t)$ obtained for PAA ($T_{g,PAA}(t) = 372.6 - 56.1 \exp\{-t/105\}$) and PEO ($T_{g,PEO}(t) = 196.15 + 33.5 \exp\{-t/92\}$) from Fig. 7(c) and data from Schönherr et al. [30], respectively, i.e.,

$$\frac{1}{T_{g,PEO-PAA}(K)} = \frac{x_{PAA}}{372.6 - 56.1e^{-t/105}} + \frac{(1-x_{PAA})}{196.15 + 33.5e^{-t/92}}. \quad (5)$$

The extended Fox relationship is plotted in Fig. 9(b) for thicknesses of 8.5 nm, 16 nm, 34.4 nm and 56 nm, corresponding to the average bilayer thicknesses for $n = 2$, 5, 8 and 40, respectively. Again, the T_g

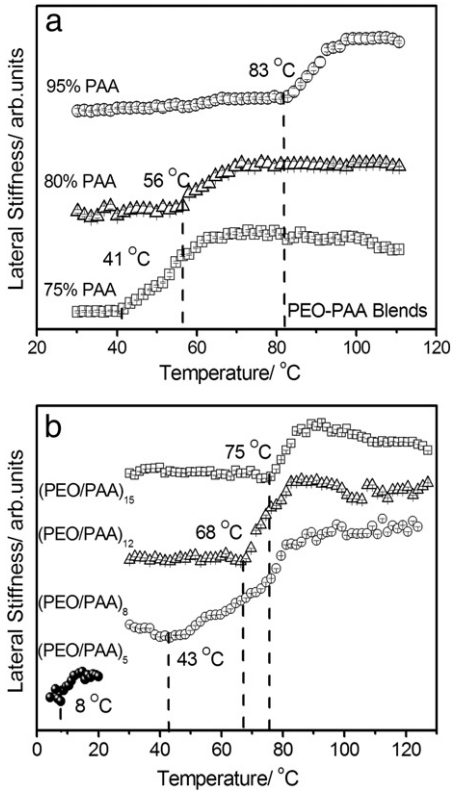

Fig. 8. SM-FM analysis of (a) PEO-PAA blends of>300 nm thickness as function of the PAA concentration, and (b) PEO/PAA LBL films as a function of the number of bilayers.

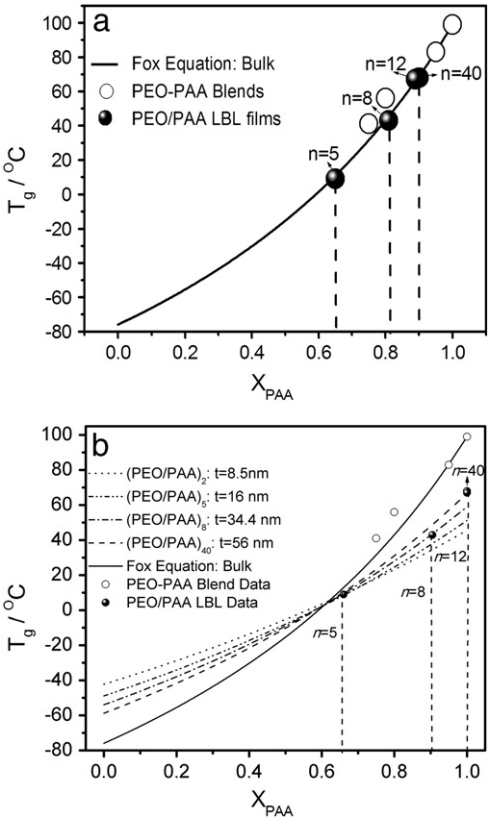

Fig. 9. Blend concentration assessment of top layer of LBL stacks based on (a) the bulk Fox fit (Eq. 4) and (b) the extended Fox fit (Eq. 5) according to the appropriate average film thickness t. The open circles represent the blend data from Fig. 8(a). The T_g values for the LBL stacks are from Fig. 8(b).

values of the LBL films, as determined in Fig. 9(b), are matched up with their PEO/PAA composition values via their thickness specific extended Fox fit, Eq. (5). The resulting x_{PAA} concentrations are distinctly increased by over 10% for $n \geq 8$, if compared to the "bulk" Fox assessment, Eq. (4). The two evaluations provide an upper and lower boundary for the concentrations of each LBL stack. If we consider that both friction and glass transition data identify the top LBL layer at around $n = 12$–15 as PAA phase (and $n > 15$), we can conclude that the extended Fox fit is the more appropriate fit for the blend concentration x_{PAA}, which reaches unity for $n = 12$ and 40.

Fig. 10 provides a compilation of the LBL concentration as function of the film's thickness and a cross-correlation with the obtained T_g values. It shows that changes in the glass transition trend-wise capture changes in the blend concentration using either of the two Fox fits. These interpretations are further supported by the direct relationship of the local glass transition and the friction coefficient (Fig. 11).

3.4. Phase heterogeneity analysis in $(PEO/PAA)_2$ LBL assembly

In contrast to the thicker LBL systems discussed above, the two-bilayer LBL films, $(PEO/PAA)_2$, revealed a variety of transition temperatures, Fig. 12(a), caused by the in-plane phase heterogeneity, as illustrated with a friction contrast map in Fig. 12(b). In the most prominent, i.e., the dark contrast region 1 of Fig. 12 (b), no transition could be observed, as indicated in the corresponding plot in Fig. 12 (a). This identifies the contrast region 1 as the PEO rich phase. It is important to note that although rich in PEO, phase 1 does not reveal a melting transition, and thus, is very effective for ionic transport. Next, the second prominent and contrast bright region 2 in Fig. 12 (b), shows a glass transition at ~12 °C

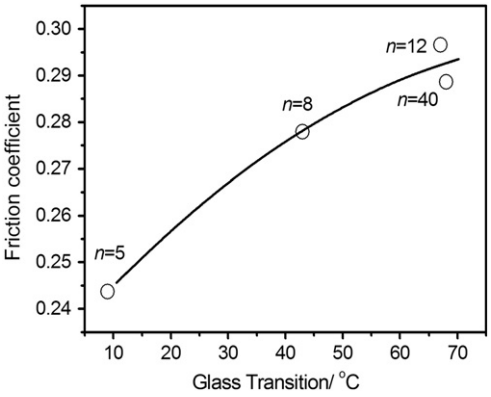

Fig. 11. Cross-correlation of the friction coefficient and the glass transition for LBL films.

similar to $(PEO/PAA)_5$, identifying it as a PAA rich region. Less pronounced are regions 3 and 4, of crystalline PEO and concentrated bulk-like PAA, respectively.

While the LBL growth process starts with a high in-plane heterogeneity of four phases, continued growth beyond the stack number of $n = 10$ manifests no in-plane phase heterogeneity, but homogeneous PEO-PAA blended layers of either PAA or PEO rich phases. The in-plane heterogeneity is captured by the exponential growth profile addressed earlier in Fig. 2, and ceases with the onset of the linear growth profile. As pointed out, the rich but amorphous PEO phases below $n = 10$ are the cause for high ionic conductivity if compared to PEO bulk systems or thick PEO-PAA LBL films, as shown in Fig. 2, approaching 10^{-7} S/cm for the two stack system.

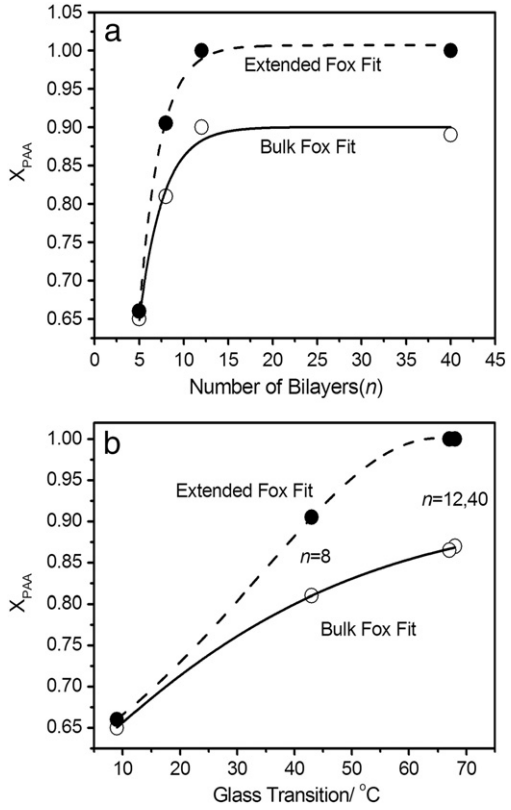

Fig. 10. (a) LBL top layer blend concentration (for bulk Fox fit and extended Fox fit) as function of the number of bilayers. (b) Cross-correlation of the glass transition values with blend concentration with increasing number of bilayers, i.e., average layer thickness.

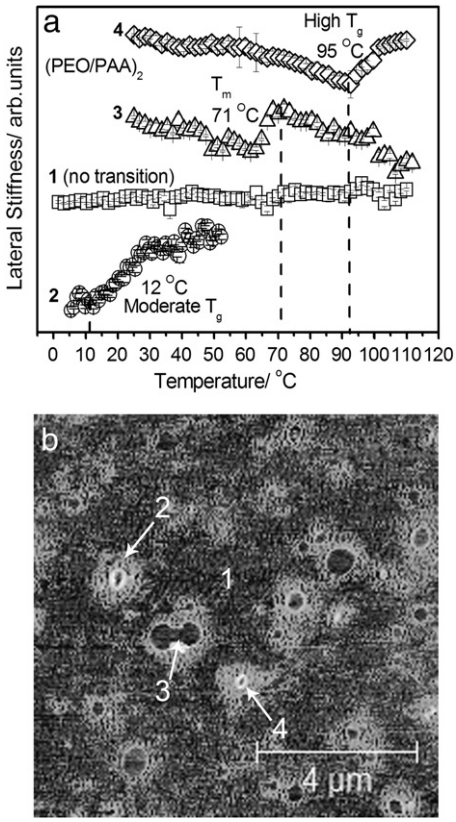

Fig. 12. $(PEO/PAA)_2$ LBL film in-plane heterogeneity (a) analyzed by SM-FM in region 1 to 4 as visualized by (b) friction contrast imaging.

4. Conclusions and outlook

With LBL stacking of PEO/PAA layers, the crystallinity within the PEO phase could be suppressed, as evidenced by increased ion conductivity. If compared to bulk PEO, an increase in the ionic conductivity up to three orders of magnitude for low stack numbers, and an order of magnitude increased saturation value of 10^{-9} S/cm for large stack numbers was found for PEO/PAA LBL assemblies. Local studies of transition properties of pure and blended phases of PEO and PAA revealed that the LBL stacking method leads to phase intermixing. Despite PAA's undesirable low ionic conductivity that is even surpassed by bulk PEO [5], the resulting ionic transport properties of PEO/PAA stacks exceeded either of the two pure components for any film thickness.

The substantial increase in ion conductivity for low stack numbers ($n<10$) is also caused by the in-plane phase heterogeneity of PEO and PAA. The existence of PEO and PAA phases within the same plane can be associated with substrate effects that reduce PEO-PAA hydrogen bonding, resulting in slow film growth and a significant in-plane PEO concentration in each plane, as observed for low stack numbers.

Also for large stacking number, we found ion conductivity values to exceed bulk PEO. This indicates that the PAA and the PEO phase are autoblended. Considering the resolution limit for our composition analysis, intermixing can be on the order of several wt.%. Autoblending throughout a single layer is possible, because of the existence of a strong driving force, i.e., PEO-PAA hydrogen bonding, and an average layer thickness of noticeably less than 100 nm.

This study also addressed the impact of interfacial constraints in the blend concentration in LBL stacks, and revealed transition shifts in pure phases of PEO and PAA. The blend ratio, as discussed by an extended Fox analysis, yielded a concentration shift from the bulk Fox analysis of up to 10%. Interestingly, for this particular blend system, the composition shift from the bulk is in favor of PAA, which is the dominating phase at the top. The shift converges to a maximum at a layer number of ~10, which corresponds to an average layer thickness of ~35 nm. As found for other thin film polymer systems, the T_g value of the pure PAA phase decreased substantially by about 55% from its bulk value to 46 °C for an 8 nm thick film. We also noted a decrease in the melting transition value of PEO by about 15% to 64 °C for 19 nm thick films, which was attributed to surface tension effects involving finite size crystal domains.

Acknowledgments

Xianke Gu thanks the China Scholarship Council for its fellowship support. D.B. Knorr thanks ARCS for a graduate fellowship.

References

[1] J.M. Tarascon, M. Armand, Nature 414 (2001) 359.
[2] A.M. Christie, S.J. Lilley, E. Staunton, Y.G. Andreev, P.G. Bruce, Nature 433 (2005) 50.
[3] J.L. Lutkenhaus, P.T. Hammond, Soft Matter 3 (2007) 804.
[4] J.L. Lutkenhaus, K.D. Hrabak, K. McEnnis, P.T. Hammond, J. Am. Chem. Soc. 127 (2005) 17228.
[5] J.L. Lutkenhaus, K. McEnnis, P.T. Hammond, Macromolecules 40 (2007) 8367.
[6] S. Sills, R.M. Overney, W. Chau, V.Y. Lee, R.D. Miller, J. Frommer, J. Chem. Phys. 120 (2004) 5334.
[7] G. Decher, Science 277 (1997) 1232.
[8] T. Cassagneau, F. Guerin, J.H. Fendler, Langmuir 16 (2000) 7318.
[9] P.K.H. Ho, J.S. Kim, J.H. Burroughes, H. Becker, S.F.Y. Li, T.M. Brown, F. Cacialli, R.H. Friend, Nature 404 (2000) 481.
[10] S. Srivastava, N.A. Kotov, Acc. Chem. Res. 41 (2008) 1831.
[11] D.M. DeLongchamp, P.T. Hammond, Langmuir 20 (2004) 5403.
[12] A.D. Taylor, M. Michel, R.C. Sekol, J.M. Kizuka, N.A. Kotov, L.T. Thompson, Adv. Funct. Mater. 18 (2008) 3003.
[13] T.R. Farhat, P.T. Hammond, Adv. Funct. Mater. 15 (2005) 945.
[14] S.Y. Yang, M.F. Rubner, J. Am. Chem. Soc. 124 (2002) 2100.
[15] W.B. Stockton, M.F. Rubner, Macromolecules 30 (1997) 2717.
[16] T. Farhat, G. Yassin, S.T. Dubas, J.B. Schlenoff, Langmuir 15 (1999) 6621.
[17] S. Lanfredi, J. Appl. Phys. 86 (1999) 2215.
[18] R.M. Overney, C. Buenviaje, R. Luginbuhl, F. Dinelli, J. Therm. Anal. Calorim. 59 (2000) 205.
[19] S. Ge, Y. Pu, W. Zhang, M. Rafailovich, J. Sokolov, C. Buenviaje, R. Buckmaster, R.M. Overney, Phys. Rev. Lett. 85 (2000) 2340.
[20] E. Meyer, L. Howald, R.M. Overney, H. Heinzelmann, J. Frommer, H.J. Guntherodt, T. Wagner, H. Schier, S. Roth, Nature 349 (1991) 398.
[21] C. Porcel, P. Lavalle, V. Ball, G. Decher, B. Senger, J.C. Voegel, P. Schaaf, Langmuir 22 (2006) 4376.
[22] T. Sreekanth, M. Jaipal Reddy, S. Subramanyam, U.V. Subba Rao, Mater. Sci. Eng. B 64 (1999) 107.
[23] X. Zheng, M.H. Rafailovich, J. Sokolov, Y. Strzhemechny, S.A. Schwarz, B.B. Sauer, M. Rubinstein, Phys. Rev. Lett. 79 (1997) 241.
[24] C. Buenviaje, S.R. Ge, M. Rafailovich, J. Sokolov, J.M. Drake, R.M. Overney, Langmuir 15 (1999) 6446.
[25] J.L. Keddie, R.A.L. Jones, R.A. Cory, Europhys. Lett. 27 (1994) 59.
[26] J.A. Forrest, J. Mattsson, Phys. Rev. E 61 (2000) R53.
[27] D.S. Fryer, P.F. Nealey, J.J. de Pablo, Macromolecules 33 (2000) 6439.
[28] K. Fukao, Y. Miyamoto, Phys. Rev. E 61 (2000) 1743.
[29] H.P. Wang, J.K. Keum, A. Hiltner, E. Baer, B. Freeman, A. Rozanski, A. Galeski, Science 323 (2009) 757.
[30] H. Schonherr, C. Frank, Macromolecules 36 (2003) 1199.
[31] R.M. Overney, E. Meyer, J. Frommer, D. Brodbeck, R. Luthi, L. Howald, H.J. Guntherodt, M. Fujihira, H. Takano, Y. Gotoh, Nature 359 (1992) 133.
[32] R.M. Overney, E. Meyer, Mater. Res. Soc. Bull. 18 (1993) 26.
[33] R.M. Overney, D.P. Leta, L.J. Fetters, Y. Liu, M.H. Rafailovich, J. Sokolov, J. Vac. Sci. Technol. B 14 (1996) 1276.
[34] J.M. Marentette, G.R. Brown, Polymer 39 (1998) 1405.
[35] E. Roduner, Chem. Soc. Rev. 35 (2006) 583.
[36] T.G. Fox, Bull. Am. Phys. Soc. 1 (1956) 22060.